Journal of Microscopy, Vol. 205, Pt 1 January 2002, pp. 53–60
Received 30 May 2001; accepted 31 July 2001

Near field optical microscopy in aqueous solution: implementation and characterization of a vibrating probe

A. MANNELQUIST*, H. IWAMOTO, G. SZABO & Z. SHAO
**Luleå University of Technology, Porsön, 971 87 Luleå, Sweden*
Department of Molecular Physiology and Biological Physics, Biophysics Graduate Program, University of Virginia School of Medicine, PO Box 800736, Charlottesville, VA 22908-0736, USA

Key words. Near field microscopy, probe design.

Summary

Near field optical microscopy (NSOM) is one of the possible solutions to circumvent the diffraction limit, but the control of the optical probe in solution has been a technical challenge for practical applications. Most recently, it has been shown that the pipette used in the scanning ion conductance microscope can be modified to form a high resolution near field optical probe. When combined with a novel distance modulation mechanism, a robust near field microscope can be constructed for operation in aqueous solution. In this paper, we present technical details of this design and a further characterization of the NSOM system for imaging in solution. Fundamental limitations of this approach in comparison to other systems are also discussed. Based on the current technology, it is concluded that better than 50 nm resolution should be achievable with this technique for fluorescence, as well as fluorescence resonance energy transfer, imaging of biological specimens.

Introduction

Since its invention, optical microscopy has made tremendous contributions to the development of science and technology. It has become an essential tool in biology and biomedicine. However, it is also well understood that as long as a lens is used to form an image or a probe, as in all conventional optical microscopes, the achievable resolution is fundamentally limited by diffraction, which cannot be circumvented even with perfect lenses (Born & Wolf, 1970). One approach to overcome this fundamental limitation is based on the concept of near field microscopy (Synge, 1928), which was first demonstrated with microwave frequencies nearly 30 years ago (Ash & Nicholls, 1972), although its extension to optical microscopy was a much more recent development (Lewis *et al.*, 1984; Pohl *et al.*, 1984; Dürig *et al.*, 1986; Harootunian *et al.*, 1986; Pohl, 1986). The rationale for near field microscopy is based on the fact that if an object is brought very close to an aperture, the illuminated area will not be much greater than the size of the aperture. Therefore, if an aperture smaller than the wavelength of the illuminating light can be fabricated and is scanned across the specimen, the spatial resolution will no longer be limited by diffraction. The resulting technique is known as near field scanning optical microscopy (Betzig *et al.*, 1987; Betzig *et al.*, 1991). Obviously, this technique should also be very attractive for biological applications where one can take advantage of the well-developed repertoire of fluorescent labels and other markers. However, a major difficulty at present is the inability to control, even with the highly successful shear force approach (Betzig *et al.*, 1991), the near field probe in aqueous solution without damage to either the probe or the soft biological specimen (Subramaniam *et al.*, 1998). Maintaining the probe position at a fixed distance from the sample surface is critical not only for avoiding damage to the probe, but also for avoiding artefactual contrast that is related to surface topography rather than fluorophore density in the case of near field fluorescence microscopy (Betzig *et al.*, 1991). Because of these difficulties, the application of the near field scanning optical microscope (NSOM) in biology has been rather limited to date (Hwang *et al.*, 1995; Moyer & Kammer, 1996; Muramatsu *et al.*, 1996; Brunner *et al.*, 1997; Keller *et al.*, 1997; Seibel & Pollack, 1997; Gheber *et al.*, 1998; Talley *et al.*, 1998).

It has been shown recently that the scanning pipette, used in the scanning ion conductance microscope (SICM) (Hansma *et al.*, 1989), can be used as a light guide to form a near field optical probe at the pulled end by rendering the pipette optically opaque with a thin layer of optically opaque material (Korchev *et al.*, 2000; Czajkowsky & Shao, 2001). As the ion current is sensitive to the distance between the opening of the pipette and the sample surface due to a partial blockage of the ion passage, this current can be used to 'lock' the pipette at a fixed distance from the sample surface with a properly configured feedback circuitry (Hansma *et al.*, 1989; Korchev *et al.*, 1997). However, preliminary experiments showed that a straightforward implementation of this idea is not as effective as expected.

Correspondence: Z. Shao. Fax: (804) 982–1616; e-mail: zs9q@virginia.edu

One of the problems is that the change in ion current is not sufficiently sensitive to tall features nearby. Therefore, during scanning, the 'tip' can often be trapped in deep 'valleys' present on the specimen surface. This is in some ways similar to the problems in atomic force microscopy when operated in the contact mode (Hansma *et al.*, 1994; Shao *et al.*, 1996). Any bending of the pipette due to this trapping, which happens easily when the pipette is pulled to submicrometre dimensions, creates an instability in the feedback circuitry because of the unexpected increase in the ion current. When this happens, the probe is forced by the feedback to crash into the specimen. In addition, the contamination of the electrodes (Ag/AgCl) can also cause a substantial drift over time (Snyder *et al.*, 1999), leading to difficulties in maintaining the probe at a fixed distance from the specimen surface. Because of these practical problems, the pipette was often operated at a 'safe' distance of several hundred nm from the specimen surface (Korchev *et al.*, 2000), leading to a lower resolution than the aperture would allow.

To circumvent these difficulties, we have recently introduced a method to modulate the distance between the pipette and the sample surface (Mannelquist *et al.*, 2001), similar to that previously used in a scanning electrochemical microscope (Wipf & Bard, 1992). The AC component created by this modulation in the ionic current is then used to control the position of the probe. At the same time, this vibration also allows the pipette to 'escape' from being trapped in surface 'valleys', a property analogous to that of the tapping mode atomic force microscope (Hansma *et al.*, 1994). In addition, the AC current is less sensitive to long-term drifts. These features have permitted the pipette to be operated at only a few nm from the sample surface, thus allowing the high-resolution ability of the scanning pipette to be utilized. In this article, we present the design and construction of a NSOM optimized for biological applications, and the results of a preliminary characterization of our prototype. Our data show that the NSOM constructed using this approach is robust and ideally suited for imaging in solution. We will also discuss the practical limitations imposed on the system by the various components, and the modifications that can be implemented to further improve/expand its performance.

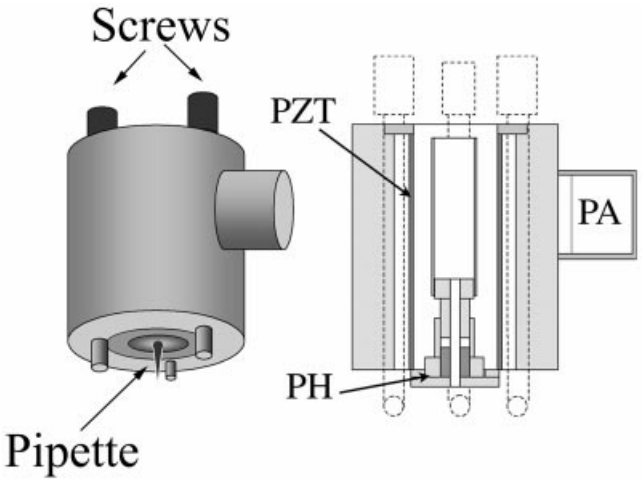

Fig. 1. Schematic illustration of the SICM/NSOM. The body of the scanner is made of heavy brass, with three fine-pitch screws tapped directly into the cylinder for levelling and approach (manual). The shielded pipette holder (PH) is mounted in the piezo tube (PZT) and the preamplifier (PA) is directly mounted on the side of the microscope to avoid electric interference and noise pickup. The shielding of the pipette from high voltage pulses imposed upon the piezo tube is critical for successful operation. The NSOM scanner is placed on top of an inverted microscope stage insulated with additional soft rubber layers.

Instrumentation

The SICM/NSOM is based on a hollow pipette filled with an electrolytic solution. A piezo tube scanner (Staveley Sensors, East Hartford, CT), 19 mm in diameter, 76 mm in length and with a thickness of 1 mm, is used to scan the pipette in three dimensions (Binnig & Smith, 1986). The scanning range is greater than $50 \times 50\ \mu m^2$ laterally and 6 μm vertically. The piezo tube is mounted on a heavy brass cylinder to ensure mechanical stability. Three fine pitch screws (80 per inch) are directly tapped into the cylinder for approach and levelling of the scanner (see Fig. 1 for an illustration). A separate piezo element is used to oscillate the specimen with a driving signal of ~180 V p-p, generated with a function generator and amplification electronics. The amplitude of oscillation can be up to 20 nm and the oscillation frequency can be set between 3 and 20 kHz. The pipette is held inside the piezo tube, and is shielded from the high voltage-scanning signal. The preamplifier (OPA2111, Burr-Brown), located on the side of the cylinder, converts the ion current to voltage, giving a sensitivity of 1 V nA^{-1} and a roll-off frequency of ~9 kHz (Fig. 2). The SICM/NSOM is placed on an inverted optical microscope (Nikon Eclipse), which is equipped with a mercury lamp and long working distance objectives. To minimize mechanical noise, the inverted microscope was placed on an air damped optical table and a 6-mm thick rubber spacer was placed between the SICM/NSOM base plate and the inverted microscope. A photomultiplier tube (PMT) (Hamamatsu R374), operated in the analogue mode, is installed directly at the video port to collect optical signal through the objective ($60\times$ at NA = 0.7), which is further sent to one of the auxiliary channels on a NanoScope IIIa controller (Digital Instruments, Santa Barbara, CA). Far field microscopy is still available through the eyepiece. The ion current is measured with Ag/AgCl electrodes (Sackmann *et al.*, 1995). The bias voltage applied is normally between 30 and 500 mV, directly set with the NanoScope IIIa controller through its STM command menu. The electrolytic solution used is 350 mM KCl in both the pipette and the sample bath. The AC signal is first converted to root-mean-square (RMS) (AD 534, Analog Devices, Novato, CA) before it is sent to the STM

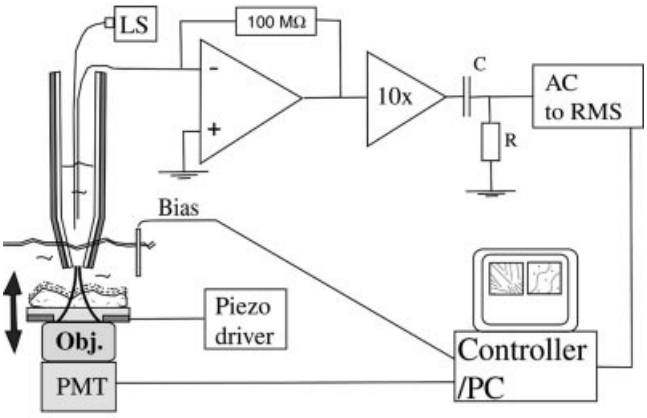

Fig. 2. Illustration of the SICM/NSOM system. Illumination is delivered by an optic fibre to the lumen of the pulled pipette from the light source (LS). Optical signal is collected through the objective (Obj) and detected by a photomultiplier tube (PMT). The sample is driven to oscillate by using a separate piezo element. The bias is set through the STM controller and the AC ion current is used as the feedback to control the z position of the pipette.

bias current input on the NanoScope IIIa controller. The light source is a 150-W quartz halogen light with a rear reflector, forming a ~5 mm spot at the focal plane. An unpolished multimode optic fibre (core diameter: 0.24 mm) is placed directly at the focal plane and the other end (unpolished) is inserted into the lumen of the pipette.

The pipettes are fabricated from thin wall quartz capillaries (1.00 mm OD and 0.70 mm ID) using a programmable CO_2 laser-based micropipette puller (P-2000, Sutter Instruments, Norwood, MA). The capillaries are usually pulled with multiple steps to make a small but robust pipette with a cone angle as great as possible in order to provide sufficient light throughput. This is critical for the present case, as the optical power available is very small. After the pipettes are pulled, they are immediately placed in a vacuum evaporator with a rotating holder. After a vacuum of 10^{-6} Torr is reached, an aluminium layer, up to 100 nm, is deposited. The pipettes are then filled by boiling in water/ethanol for 10–15 min and then backfilled with 350 mM KCl. One hour is normally required for sufficient diffusion to occur. Before filling, the integrity of the aluminium coating is examined with a light microscope and the quality of the pipette is examined with a scanning electron microscope (SEM). A typical pipette after coating is shown in Fig. 3. The optical aperture is less than 200 nm.

To make a standard test sample, 8–12 µL of 0.25% 2.2 µm polystyrene beads (Bangs Laboratories, Fishers, IN) are placed on cleaned cover glass and allowed to dry in air. After all solution is evaporated, the beads are closely packed on the glass surface. Then a thin film of aluminium, < 20 nm, is deposited in a vacuum evaporator. The beads are subsequently removed by sonication in water for 20 min. An optical image of such a test sample is shown in Fig. 4.

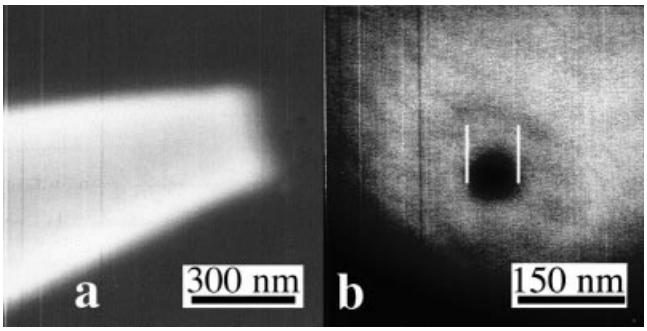

Fig. 3. SEM images of pulled quartz pipettes. (a) An uncoated pipette is viewed from the side at low voltage. (b) A coated pipette with a ~100 nm layer of aluminium is viewed from the front. The well-defined 60 nm opening in the pipette is clearly seen.

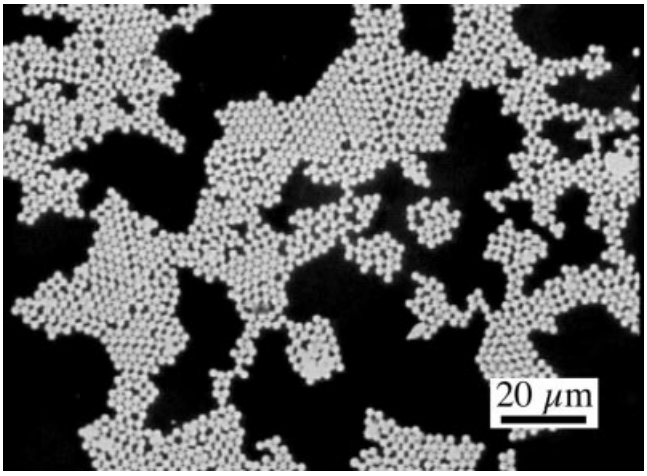

Fig. 4. Optical image of a deposited aluminium mask of closely packed 2.2 µm polystyrene beads on a glass surface. These are the standard samples used for the characterization of NSOM performance.

Results and discussion

In order to use the ion current through the quartz pipette as the feedback signal to control the position of the near field probe, the current vs. distance relationship must be well characterized. As shown by Schwab (1990) and others (Korchev *et al.*, 1997; Nitz *et al.*, 1998), this ion current has a relatively simple relationship to the distance, which can be described by the following equation:

$$I = \frac{U}{R_P}\left\{1 + \frac{1.5 \cdot \ln(r_a/r_i) \cdot r_0 \cdot r_i}{L_p \cdot z}\right\}^{-1} \qquad (1)$$

where U is the bias voltage, R_p the pipette resistance, r_a/r_i the ratio between outer and inner radius at the end of the pulled pipette, r_0 the inner radius near the electrode which is at a distance L_p from the pipette opening, and z the distance from the pipette opening to the sample surface. In this case, the shape of

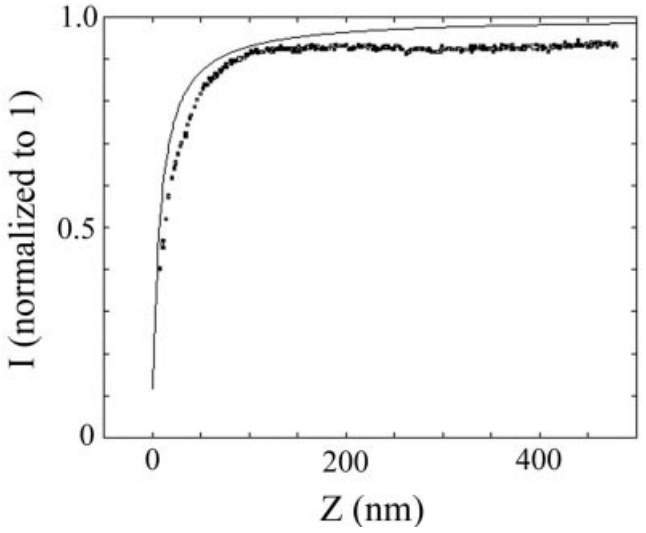

Fig. 5. Ionic current vs. distance. The solid line shows the ion current for a 100 nm pipette as a function of the mean distance from the sample, calculated by Eq. (1). The dotted line shows the actual measurements. The two curves agree reasonably well.

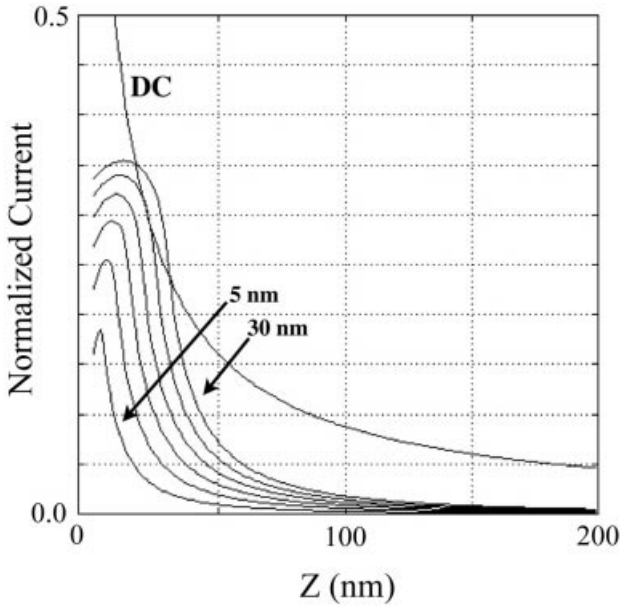

Fig. 6. Theoretical calculations of DC and AC currents for a pipette 200 nm in diameter. The RMS average of the AC current is calculated for oscillation amplitudes of 5–30 nm. Clearly, the sensitivity is greater for the AC current due to its greater slope. The DC current is inverted to make the comparison.

the probe is assumed to be conical, a reasonable assumption based on SEM measurements (Fig. 3). It is noted that at a distance far away from the sample surface, the ion current is constant, as described in standard electrophysiology textbooks (Sackman & Neher, 1995). The current starts to decrease when the opening of the pipette begins to experience the blockage by the sample surface. In Fig. 5, the measured ion current is shown with the curve derived from Eq. (1). It is seen that the theoretical description, despite its simplicity, agrees reasonably well with the experimental data. It is important to note that the aluminium coating, which is electronically floating, does not have a significant effect on the ion current, as demonstrated by approach curves. This is critical because were the current significantly altered by the metal coating, it would be difficult to use the ion current to sense the distance between the probe and the specimen surface.

When the distance z becomes time variable, i.e. the sample or the pipette is driven to oscillate at a fixed amplitude δ, we can substitute $z = z_0 + \delta \sin \omega_0 t$ into Eq. (1). Then we can expand the equation according to δ to decompose Eq. (1) into a DC offset and a series of periodic (AC) terms:

$$I = I_0 \left\{ \frac{z_0}{z_0 + k} + \delta \cdot \frac{k \cdot \sin(\omega_0 \cdot t)}{(z_0 + k)^2} - \delta^2 \cdot \frac{k \cdot \sin^2(\omega_0 \cdot t)}{(z_0 + k)} + \ldots \right\} \quad (2)$$

where

$$k = \frac{1.5 \cdot \ln(r_a / r_i) \cdot r_0 \cdot r_i}{L_p} \quad (3)$$

and

$$I_0 = \frac{U}{R_P} \quad (4)$$

Retaining only the first AC term, we obtain a very simple relationship for the RMS component of the signal:

$$RMS = I_0 \cdot \frac{1}{\sqrt{2}} \cdot \frac{\delta \cdot k}{(z_0 + k)^2} \quad (5)$$

In comparison to Eq. (1), the *RMS* signal is clearly more sensitive to the distance (z_0) than the static term at the same average distance z_0. Normally k is a small number; for example, for a small pipette, one may have $r_i = 25$ nm, $r_a = 50$ nm, $L_p = 25$ mm and $r_o = 0.35$ mm. In this case, k is about 0.4 nm. The AC current is clearly suited for the use as feedback control of the probe position and should provide a better performance than the straightforward ion current. A theoretical comparison between the RMS average with different oscillation amplitudes, δ, and the DC current (inverted) is plotted in Fig. 6. The effective range of the AC current is apparently much shorter than that of the DC current, which should be more suited for improving the spatial resolution. In addition, when the (mean) distance is too close to the specimen surface, the pipette opening can be completely blocked for part of the oscillation cycle. Therefore, no current could flow for this part of the cycle, which is responsible for the reduction of the AC current at very small distances. This is certainly a situation that needs to be avoided in practice. But for most applications, the probe would

have been broken before reaching this regime. From this point of view, the practical implications are not as serious as one might have assumed.

As the (*RMS*) AC current has a monotonically increasing relationship with the distance, an additional advantage is that the AC current can be used directly with an STM controller without the need for a null current (Korchev *et al.*, 1997). It is also clear that slow drifts in the electronics and the electrodes should have only minor effects on the stability of imaging in this case. Moreover, the shorter interaction range should allow the pipette to be placed just a few nm above the surface, thus making the NSOM fully compatible with fluorescence resonance energy transfer (FRET) microscopy (Stryer, 1978; Vickery & Dunn, 1999).

In a practical imaging system, the oscillation frequency useable is normally limited by the time response of the pre-amplifier used to convert the ion current into voltage. As the current through the pipette can be as small as a few pA, especially for pipettes 20–50 nm in diameter, the gain of the preamplifier (current to voltage converter) must be set very high so that the distributed capacitance limits the useable frequency response to less than 10 kHz. As significant improvement over this range is normally quite difficult to achieve, all of our experiments used 8–9 kHz. As several cycles of oscillation would be required for a reliable interpretation of the 'mean' current, a 0.5 ms pixel time would have 4–5 complete cycles, which appears to be the practical limit on the frame time with this approach. For an image of 64×64 pixels, the frame time would be about 2 s. For faster data acquisition, line scans may have to be used, and this has been demonstrated with AFM when examining dynamic processes in real time (Viani *et al.*, 2000). However, it is important to consider that in most NSOM systems, the pixel time is most likely dictated by the amount of light available (Gustafsson *et al.*, 1998), rather than the response of the feedback system. In fact, much longer pixel times were often required for a sufficient signal-to-noise ratio for other NSOM applications.

To characterize the performance of the system, we have used a 150 W halogen lamp as the light source. When the optic fibre is placed onto the focused spot of the lamp, the measured transmitted light at the other end of the fibre is only about 60 μW. The efficiency of light transmission through the pipette (aperture) is also directly measured when the optic fibre (unpolished) is inserted into the electrolyte-filled aluminium coated pipette. These results are shown in Fig. 7, where the diameter of the pipette is measured with a SEM. Interestingly, the measured transmittance for a 100 nm pipette is about 10^{-6}, which is about 10 times higher than other types of NSOM probes with a cone angle of ~23° (Hecht *et al.*, 2000). The reason for the slightly higher efficiency is not yet clear. It is also interesting to note that the transmitted light power scales as $\sim a^3$, where a is the aperture size (Mannelquist *et al.*, 2001). This is also different from the Bethe–Bouwkamp model where the expected transmission coefficient should scale as $\sim a^4$ for a

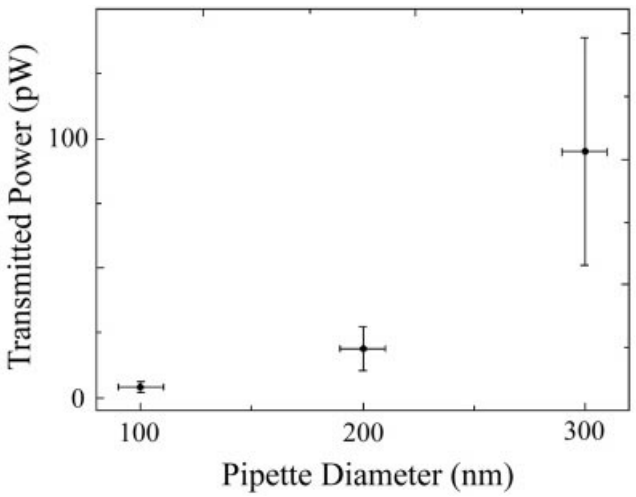

Fig. 7. Transmitted optical power vs. the diameter of aluminium-coated pipettes with a cone angle around 23°, estimated from SEM images. The optical power delivered to the pipette is ~ 60 μW. The overall attenuation is between $\sim 10^{-6}$ and 10^{-8} depending on the size of the pipette.

subwavelength aperture (Bethe, 1944; Bouwkamp, 1950). A more detailed theoretical modelling will be needed to provide useful insights on these issues.

The optical signal is collected through a long working distance objective (60×) with a numerical aperture of 0.7 by the PMT installed at the video port. As the PMT is operated in the analogue mode, the equivalent dark count is $\sim 5 \times 10^7$ s^{-1} at the maximum gain, including contributions from the built in preamplifier. For a pixel time of 1 ms, this gives $\sim 5 \times 10^4$ counts. For a 200 nm pipette, the total number of photons emitted through the probe (aperture) is about $\sim 3 \times 10^4$ in 1 ms for our system (see Fig. 7). But, as only 10–20% of the emitted photons is collected, the signal-to-noise ratio, which can be estimated as:

$$S/N = \frac{n \cdot \alpha}{\sqrt{d_c + n \cdot \alpha}} \qquad (6)$$

would be around 20, where n is the number of emitted photons, α the collection efficiency of the optical system and d_C the dark count. This should be sufficient for obtaining good quality NSOM images.

We have applied this method to image a test sample previously imaged with transmission optical microscopy, in order to demonstrate the feasibility of this approach and to confirm the practical limits estimated based on theoretical considerations. A typical example is shown in Fig. 8, where topographic images (obtained with ion current) and NSOM images are acquired simultaneously. At a large scale (Fig. 8(a) and (b)), the pattern formed by the closely packed micro beads is clearly resolved. In the topographic images (Fig. 8a), the deposited aluminium appears as isolated spots, and the same spot appears to be optically dark in the NSOM image (Fig. 8b). The general features of these images correspond to each other very well.

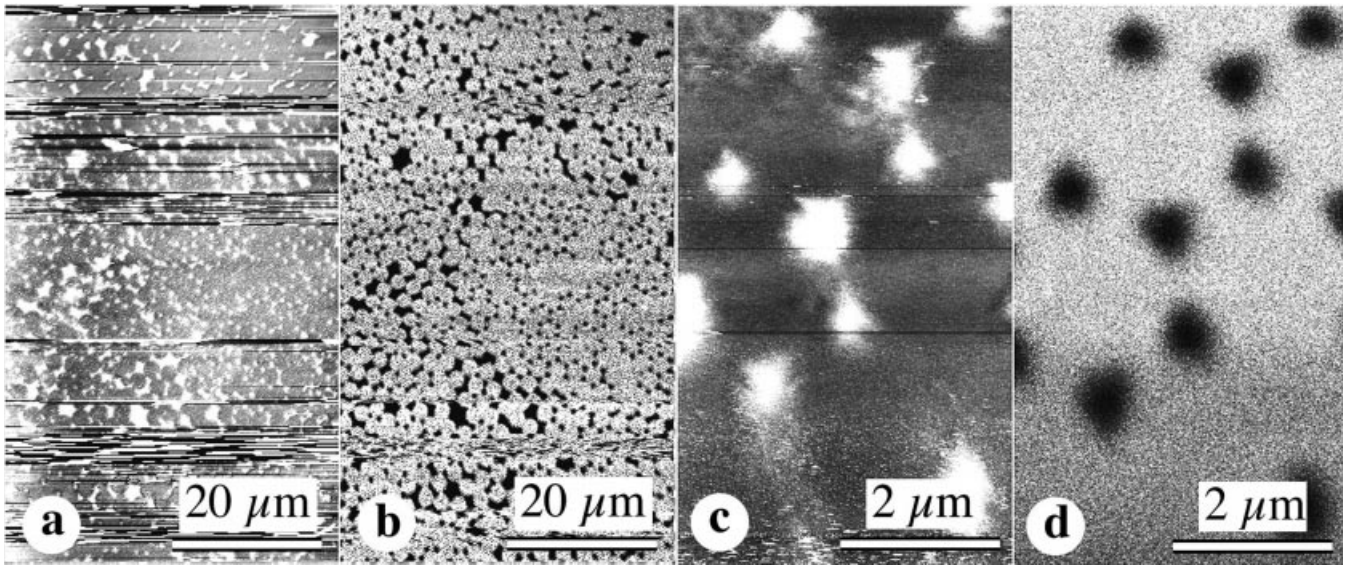

Fig. 8. Simultaneous SICM and NSOM images. Topographic images are shown in (a) and (c) and NSOM images are shown in (b) and (d). Pixel time was 2 ms (scan speed 0.5 Hz). The deposited aluminium pattern formed by the closely packed micro beads is clearly resolved both topographically and optically. The resolution in (d) is estimated to be 200–300 nm from the edge of the resolved features. This resolution is consistent with the size of the probe used. More features seem to be resolved in the SICM image (c), most likely due to local protrusions at the end of the pipette (see text). In general, the NSOM images correspond well with the SICM images.

At a smaller scan size (Fig. 8(c) and (d)), the resolution can be estimated from the edge of the resolved features by defining the resolution as the width between the lower 10% and the upper 10% of the near-field signal at the edge. Based on this definition, the estimated resolution is ~200–300 nm. This is consistent with the estimated aperture size based on SEM measurements. It is noted that the NSOM image is well defined and relatively clean, indicating that the aperture is well formed. However, it is also noted that more features seemed resolvable in the topographic image, as in other NSOM systems. The obvious explanation of this observation is that the end of the pipette could have protrusions from the nominal surface of the ruptured end. When the probe is very close to the surface, these protrusions could have caused a sufficient reduction in the current while scanning over a surface feature, as substantial blockage of the ion passage is not required for imaging. Therefore, the apparent resolution can be higher than the nominal size of the probe in the SICM image. In fact, occasionally aligned fine features have been observed, almost certainly caused by multiple protrusions at the end of the probe. As expected, such protrusions have no effect on the optical image because they are transparent.

The signal-to-noise ratio (S/N) can also be estimated directly from optically transparent, aluminium free regions. For a pixel time of 1 ms (Fig. 9a), the estimated S/N is ~10, as defined by the mean signal divided by *rms* noise calculated from the pixels. When the pixel time is increased to 2 ms (Fig. 9b), the estimated S/N is improved to ~15. Although this relationship (scaling) is similar to that predicted by Eq. (6), the exact S/N is lower than

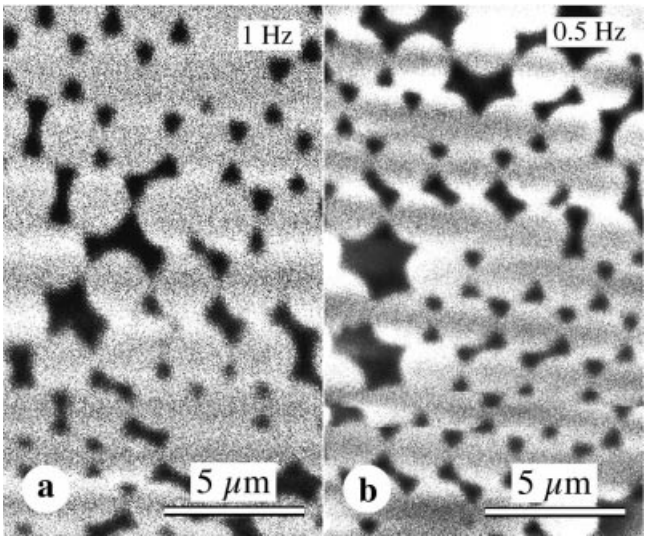

Fig. 9. Evaluation of signal-to-noise ratio in the NSOM image. (a) 1 ms pixel time (1 Hz scan speed). (b) 2 ms pixel time (0.5 Hz scan speed). Signal-to-noise ratio is excellent for both images, which can be estimated from aluminium-free regions in the image (see text).

anticipated. The discrepancy from the predicted value may be attributed to other sources of noise that are not included in Eq. (6), such as the ambient background, and instabilities in the lamp, among others. These measurements also indicate that the current set-up can be further optimized in order to improve the signal-to-noise ratio. However, for smaller pipettes,

a higher illumination power and/or a more efficient detection system will be required.

As the ultimate goal is to achieve high resolution fluorescence microscopy for biological applications, it is important to understand the fundamental limits and estimate what improvements would be necessary in order to achieve this goal. Clearly, the current detection limit can be much improved. The most obvious solution is to use a photon counting PMT, which can have a dark count much less than 10 ms^{-1} at ambient temperature. Assuming that all electronic noise, such as readout noise, etc., can be rendered insignificant, a signal-to-noise ratio of 10 for a 1 ms pixel time would require ~110 photons to be collected, if we assume 10 dark counts in 1 ms (an overestimate). As even for a NA = 1.4 objective, only 20–30% of total emitted photons can be collected, we would need to have ~600 fluorescence photons from the fluorophores in the illuminated volume (~ 0.2 pW), allowing an additional loss due to the various optical surfaces and the bandpass filter. The number of fluorophores (N) detectable under this condition can be estimated by rewriting and simplifying the Beer–Lambert law (Cantor & Schimmel, 1980) as the following:

$$N = \frac{P \cdot N_A \cdot A}{\varepsilon \cdot \Phi \cdot P_0} \tag{7}$$

where P is the minimum detectable power (W), N_A is the Avogadro constant (M^{-1}), A the illuminated area (for simplicity, the size of the aperture of the pipette can be used (dm^2)), ε the extinction coefficient ($M^{-1}\ dm^{-1}$), which can be assumed to be 2×10^6 for most cases, Φ the quantum efficiency (~0.8) and P_0 the illumination from the pipette (W). For P = 1 nW, P_0 = 0.2 pW, we have N = 15. In other words, 15 fluorophores will be needed in the illuminated area (volume), in order to have the required S/N of 10. As up to six fluorophores can be attached to a single antibody, this requirement should be practical for a pipette as small as 50 nm. Three or four antibodies will be required in this area. As this is still far below the photobleaching limit of many fluorophores, a higher illumination power can be tolerated for a shorter pixel time or fewer fluorophores. 1 nW total light output from the aperture should be achievable with available intermediate power lasers. As the pipette is fully immersed in aqueous solution, damage to the aluminium coating due to laser heating (Stähli*n et al.*, 1996) should be a minor problem. It is important to note that these calculations have assumed a zero background. Therefore, for a measurable background, the contrast will be reduced, which may require a longer pixel time to compensate.

Another aspect that may be improved is that in the current set-up, the pipette is continuously illuminated. As such, when the pipette is at the furthest point of the oscillation cycle, the illuminated area is greater than that at the closest point to the sample surface. For small oscillation amplitudes, this would impose a minor effect, but for larger amplitudes that may be needed for topographically rough surfaces, the illumination can be gated in synchrony with the oscillation, so that the pipette will emit light only when it comes close to the sample surface.

As in any other form of probe microscopy, the absolute resolution will have to be determined by the smallest pipettes that can be pulled that can still be filled with electrolyte. Fortunately, published literature has shown that pipettes down to 20 nm can be made and filled with electrolytes (Frank & Becker, 1964). However, at such small dimensions, evanescent penetration into the metal coating must also be considered, which can be comparable to the size of the aperture (Lieberman *et al.*, 1990). Given this fundamental limitation, the achievable resolution with this approach appears to be in the range 30–40 nm. Pipettes much smaller than this, even if they can be filled with electrolytes, are unlikely to further improve the resolution. However, attaching a nano-crystal to the end of the pipette may achieve a higher resolution, but the lifetime of even nano-crystals under such intense illumination needs to be carefully determined.

Conclusions

Unlike most other NSOM systems, the design presented in this article uses a vibrating, metal-coated pipette to form the scanning optical probe and the AC ionic current to control the position of this probe. Our data show that this novel scheme can overcome most of the difficulties encountered by other approaches when applied in solution and can provide a robust and reliable imaging platform. Our analysis, based on commonly available components, also indicates that with further optimization in signal collection, the optical resolution should be able to reach the sub-100 nm range. Not only is this design compatible with normal far field imaging, FRET (Lakowicz, 1983) can also be implemented, as well as two photon excitation (Denk *et al.*, 1990; Piston *et al.*, 1992; Jenei *et al.*, 1999) with near IR illumination.

Acknowledgements

This work was supported by grants from US National Institutes of Health, US National Science Foundation (to Z.S.), Swedish Institute, Hans Whertén Foundation and Wallenberg Foundation (to A.M.). The authors also thank Mr Gang Huang for technical assistance, Dr D. Medich for helpful discussions and Professor S. Fredriksson for support.

References

Ash, E.A. & Nicholls, G. (1972) Super-resolution aperture scanning microscope. *Nature*, **237**, 510–512.

Bethe, H. (1944) Theory of diffraction by small holes. *Phys. Rev.* **66**, 163–182.

Betzig, E., Isaacson, M. & Lewis, A. (1987) Collection mode near-field optical microscopy. *Appl. Phys. Lett.* **51**, 2088–2090.

Betzig, E., Trautman, J.K., Harris, T.D., Weiner, J.S. & Kostelak, L.R. (1991) Breaking the diffraction barrier: optical microscopy on a nanometric scale. *Science*, **251**, 1468–1470.

Binnig, G. & Smith, D.P.E. (1986) Single-tube three-dimensional scanner for scanning tunneling microscopy. *Rev. Sci. Instrum.* **57**, 1688–1689.

Born, M. & Wolf, E. (1970) *Principles of Optics*, 2nd edn. Pergamon, Oxford.

Bouwkamp, C.J. (1950) On Bethe's theory of diffraction by small holes. *Philips Res. Report*, **5**, 321–332.

Brunner, R., Bietsch, A., Hollricher, O. & Marti, O. (1997) Distance control in near-field optical microscopy with piezoelectrical shear-force detection suitable for imaging in liquids. *Rev. Sci. Instrum.* **68**, 1769–1772.

Cantor, C.R. & Schimmel, P.R. (1980) *Biophysical Chemistry*. Freeman, New York.

Czajkowsky, D.M. & Shao, Z. (2001) Localizing ion channels in biological membranes with scanning probe microscopy: a perspective. *Ion Channel Localization Methods and Protocols* (ed. by A. Lopatin and C. Nichols), pp. 461–481. Humana, Totowa, NJ.

Denk, W., Strickler, J.H. & Webb, W.W. (1990) Two-photon laser scanning fluorescence microscopy. *Science*, **248**, 73–76.

Dürig, U., Pohl, D. & Rohner, F. (1986) Near-field optical scanning microscopy with tunnel-distance regulation. *IBM. J. Res. Dev.* **30**, 478–483.

Frank, K. & Becker, M.C. (1964) *Physical Techniques in Biological Research*, Vol. 5. Academic Press, London.

Gheber, L.A., Hwang, J. & Edidin, M. (1998) Design and optimization of a near-field scanning optical microscope for imaging biological samples in liquid. *Appl. Optics*, **37**, 3574–3581.

Gustafsson, A., Pistol, M.E., Montelius, L. & Samuelson, L. (1998) Local probe techniques for luminescence studies of low-dimensional semiconductor structures. *J. Appl. Phys.* **84**, 1715–1775.

Hansma, P.K., Cleveland, J.P., Radmacher, M., Walters, D.A., Hillner, P.E., Bezanilla, M., Fritz, M., Vie, D., Hansma, H.G., Prater, C.B., Massie, J., Fukunaga, L., Gurley. J. & Elings, V. (1994) Tapping mode atomic force microscopy in liquids. *Appl. Phys. Lett.* **64**, 1738–1740.

Hansma, P.K., Drake, B., Marti, O., Gould, S.A.C. & Prater, C.B. (1989) The scanning ion-conductance microscope. *Science*, **243**, 641–643.

Harootunian, A., Betzig, E., Isaacson, M. & Lewis, A. (1986) Super-resolution fluorescence near-field scanning optical microscopy. *Appl. Phys. Lett.* **49**, 674–676.

Hecht, B., Sick, B., Wild, U.P., Decker, V., Zenobi, R., Martin, O.J.F. & Pohl, D.W. (2000) Scanning near-field optical microscopy with aperture probes: fundamentals and applications. *J. Chem. Phys.* **112**, 7761–7774.

Hwang, J., Tamm, L.K., Bohm, C., Ramalingam, T.S., Betzig, E. & Edidin, M. (1995) Nanoscale complexity of phospholipid monolayers investigated by near-field scanning optical microscopy. *Science*, **270**, 610–614.

Jenei, A., Kirsch, A.K., Subramaniam, V., Arndt-Jovin, D.J. & Jovin, T.M. (1999) Picosecond multiphoton scanning near-field optical microscopy. *Biophys. J.* **76**, 1092–1100.

Keller, T.H., Rayment, T., Klenerman, D. & Stephenson, R.J. (1997) Scanning near-field optical microscopy in reflection mode imaging in liquid. *Rev. Sci. Instrum.* **68**, 1448–1454.

Korchev, Y.E., Bashford, L., Milovanovic, M., Vodyanoy, I. & Laboratory, M. (1997) Scanning ion conductance of living cells. *Biophys. J.* **73**, 653–658.

Korchev, Y.E., Raval, M., Laboratory, M., Gorelik, J., Edwards, C.R.W., Rayment, T. & Klenerman, D. (2000) Hybrid scanning ion conductance and scanning near-field optical microscopy for the study of living cells. *Biophys. J.* **78**, 2675–2679.

Lakowicz, J.R. (1983) *Principles of Flourescence Spectroscopy*. Plenum, New York.

Lewis, A., Isaacson, M., Harootunian, A. & Muray, A. (1984) Development of a 500 Å resolution light microscope. I. Light is efficiently transmitted through $\lambda/16$ diameter aperture. *Ultramicroscopy*, **13**, 227–231.

Lieberman, K., Harush, S., Lewis, A. & Kopelman. R. (1990) A light source smaller than the optical wavelength. *Science*, **247**, 59–61.

Mannelquist, A., Iwamoto, H., Szabo, G. & Shao, Z. (2001) Near field optical microscopy with a vibrating probe in aqueous solution. *Appl. Phys. Lett.* **78**, 2076–2078.

Moyer, P.J. & Kammer, S.B. (1996) High-resolution imaging using near-field scanning optical microscopy and shear force feedback in water. *Appl. Phys. Lett.* **68**, 3380–3382.

Muramatsu, H., Chiba, N., Homma, K., Ataka, T., Ohta, S., Kusumi, A. & Fujihira, M. (1996) Scanning near-field optic/atomic force microscopy in liquids. *Thin Solid Films*, **273**, 335–338.

Nitz, H., Kamp, J. & Fuchs, H. (1998) A combined scanning ion-conductance and shear-force microscope. *Probe Microsc.* **1**, 187–200.

Piston, D.W., Sandison, D.R. & Webb, W.W. (1992) Time-resolved fluorescence imaging and background rejection by two-photon excitation in laser scanning microscopy. *Proc. SPIE*, **1640**, 379–390.

Pohl, D. (1986) US Patent. 4,604,520.

Pohl, D., Denk, W. & Lanz, M. (1984) Optical stethoscopy: image recording with resolution $\lambda/20$. *Appl. Phys. Lett.* **44**, 651–653.

Sackmann, B. & Neher, E. (1995) *Single Channel Recording*, 2nd edn. Plenum, New York.

Schwab, E. (1990) Aufbau und Erprobung eines Raster-Ionen-Leitungs-mikroskops (RILM). Diploma Thesis, Physikalisches Institut, Münster.

Seibel, E.J. & Pollack, G.H. (1997) Imaging 'intact' myofibrils with a near-field scanning optical microscope. *J. Microsc.* **186**, 221–231.

Shao, Z., Mou, J., Czajkowsky, D.M., Yang, J. & Yuan, J.Y. (1996) Biological atomic force microscopy: what is achieved and what is needed. *Adv. Phys.* **45**, 1–86.

Snyder, K.V., Krigstein, A.M. & Sachs, F. (1999) A convenient electrode holder for glass pipettes to stabilize electrode potentials. *Eur. J. Physiol.* **438**, 405–411.

Stählin, M., Bopp, M.A., Tarrach, G., Meixner, A.J. & Zschokke-Gränacher, I. (1996) Temperature profile of fiber tips used in scanning near-field optical microscopy. *Appl. Phys. Lett.* **68**, 2603–2605.

Stryer, L. (1978) Fluorescence energy transfer as a spectroscopic ruler. *Ann. Rev. Biochem.* **47**, 819–846.

Subramaniam, V., Kirsch, A.K. & Jovin, T.M. (1998) Cell biological applications of scanning near-field optical microscopy (SNOM). *Cell. Mol. Biol.* **44**, 689–700.

Synge, E.H. (1928) A suggested model for extending microscopic resolution into the ultra-microscopic region. *Philos. Mag.* **6**, 356–362.

Talley, C.E., Lee, M.A. & Dunn, R.C. (1998) Single molecule detection and underwater fluorescence imaging with cantilevered near-field fiber optic probes. *Appl. Phys. Lett.* **72**, 2954–2956.

Viani, M.B., Pietrasanta, L.I., Thompson, J.B., Chand, A., Gebeshuber, I.C., Kindt, J.H., Richter, M., Hansma, H.G. & Hansma, P.K. (2000) Probing protein-protein interactions in real time. *Nat. Struct. Biol.* **7**, 644–647.

Vickery, S.A. & Dunn, R.C. (1999) Scanning near-field fluorescence resonance energy transfer microscopy. *Biophys. J.* **76**, 1812–1818.

Wipf, D.O. & Bard, A.J. (1992) Scanning Electrochemical Microscopy 15: Improvements in imaging via tip-position modulation and lock-in detection. *Anal. Chem.* **64**, 1362–1367.